Inorg. Chem. **2007**, *46*, 7005–7011

Synthesis, Structure, Characterization, and Calculations of Two New Sn^{2+}–W^{6+}–oxides, Sn_2WO_5 and Sn_3WO_6

Hong Young Chang, Kang Min Ok, Jun Ho Kim, and P. Shiv Halasyamani*

Department of Chemistry and Center for Materials Chemistry, 136 Fleming Building, University of Houston, Houston, Texas 77204-5003

Matthew Stoltzfus and Patrick Woodward

Department of Chemistry, The Ohio State University, 100 West 18th Avenue, Columbus, Ohio 43210

Received April 18, 2007

Two new Sn^{2+}–W^{6+}–oxides, Sn_2WO_5 and Sn_3WO_6, have been synthesized hydrothermally, and their structures have been determined by single-crystal X-ray diffraction methods. Both materials exhibit layered structural topologies consisting of two edge-shared WO_6 octahedra connected to SnO_3 and SnO_4 polyhedra. Both the W^{6+} and Sn^{2+} cations are in locally asymmetric coordination environments attributable to second-order Jahn–Teller effects. Infrared and Raman spectroscopy, UV–vis diffuse reflectance spectroscopy, and thermogravimetric analysis were also performed on the reported materials. Theoretical calculations using the tight binding linear muffin tin orbital method agree with the observed electronic properties of these materials and indicate that the stereoactive lone pair on the Sn^{2+} is similar for both materials. Crystal data: Sn_2WO_5, monoclinic, space group $P2_1/n$ (No. 14), $a = 7.994(2)$ Å, $b = 13.712(4)$ Å, $c = 10.383(3)$ Å, $\beta = 110.507(3)°$, $V = 1066.0(5)$ Å^3, and $Z = 4$; Sn_3WO_6, monoclinic, $C2/c$ (No. 15), $a = 12.758(3)$ Å, $b = 8.0838(16)$ Å, $c = 13.865(3)$ Å, $\beta = 112.49(3)°$, $V = 1321.2(5)$ Å^3, and $Z = 8$.

Introduction

Metal cation distortions in oxides, specifically, octahedrally coordinated d^0 transition metals and lone-pair cations, play a critical role in a variety of technologically important physical properties such as second-harmonic generation, piezoelectricity, and ferroelectricity.[1−3] With both families of cations, the structural distortions are thought to be attributable to second-order Jahn−Teller (SOJT) effects.[4−10] For the octahedrally coordintated d^0 transition metals, SOJT effects occur when the empty d-orbitals of the metal mix with the filled p-orbitals of the oxide ligands. The SOJT effects results in the d^0 cation displacing from the center of its oxide octahedron along one of three special directions, vertex, face, or edge, the local C_4, C_3, or C_2 direction, respectively, or toward an intermediate direction between the special directions.[11] With the lone-pair cations, a somewhat more complicated situation is observed.[12,13] We define a lone-pair cation as one of the following, Se^{4+}, Sn^{2+}, Sb^{3+}, Te^{4+}, I^{5+}, Tl^{+}, Pb^{2+}, or Bi^{3+}. While there is an extensive debate in the literature on the exact orbital character of the lone-pair,[14−20] there is no question that these cations generally exhibit asymmetric coordination environments.

An important question that is not fully understood is how the presence of asymmetric lone-pair polyhedra impact the SOJT distortions of d^0 transition metal ions. Recently one

* To whom correspondence should be addressed. E-mail: psh@uh.edu.

(1) Cady, W. G. *Piezoelectricity: An Introduction to the Theory and Applications of Electromechanical Phenomena in Crystals*; Dover: New York, 1964.
(2) Jona, F.; Shirane, G. *Ferroelectric Crystals*; Pergamon Press: Oxford, U.K., 1962.
(3) Lang, S. B. *Sourcebook of Pyroelectricity*; Gordon & Breach Science: London, 1974.
(4) Opik, U.; Pryce, M. H. L. *Proc. R. Soc. London, Series A* **1957**, *A238*, 425.
(5) Bader, R. F. W. *Mol. Phys.* **1960**, *3*, 137.
(6) Bader, R. F. W. *Can. J. Chem.* **1962**, *40*, 1164.
(7) Pearson, R. G. *J. Am. Chem. Soc.* **1969**, *91*, 4947.
(8) Pearson, R. G. *THEOCHEM* **1983**, *103*, 25.
(9) Wheeler, R. A. W., M.-H.; Hunghbanks, T.; Hoffmann, R.; Burdett, J. K.; Albright, T. A. *J. Am. Chem. Soc.* **1986**, *108*, 2222.
(10) Kunz, M. B.; David, I. *J. Solid State Chem.* **1995**, *115*, 395.
(11) Goodenough, J. B. *Annu. Rev. Mater. Sci.* **1998**, *28*, 1.
(12) Gillespie, R. J.; Nyholm, R. S. *Q. Rev., Chem. Soc.* **1957**, *11*, 339.
(13) Orgel, L. E. *J. Chem. Soc.* **1959**, 3815.

10.1021/ic700740m CCC: $37.00
Published on Web 07/21/2007

of us examined all of the structurally well-characterized oxides that contain an octahedrally coordinated d^0 transition metal and a lone-pair cation.[21] Surprisingly, fewer than 90 of these types of oxides have been reported. We determined that when the d^0 transition metal displaced from the center of its oxide octahedron, the direction of this distortion always resulted in a lengthening of the bonds to oxide ligands that also formed bonds with a lone-pair cation. We argued that the directionality of the d^0 transition metal distortion is attributable to the structural inflexibility of the lone-pair polyhedra.

With regard to compounds containing lone-pair cations and d^0 cations, there are a number of substantial "gaps" in the possible combinations. For example, no oxide materials have been reported where Sb^{3+} is present in combination with either Ti^{4+}, Zr^{4+}, Hf^{4+}, or V^{5+}. There are also very few examples of Sn^{2+} ions being found in combination with d^0 transition metal ions. In fact, only α- and β-$SnWO_4$ have been reported.[22,23] The dearth of oxide compounds containing Sn^{2+} and a d^0 cation may be attributed to the tendency for SnO to disproportionate at elevated temperatures to Sn^0 and SnO_2. In this paper, we report on the synthesis, structure, characterization, and electronic structure calculations of two new $Sn^{2+}-W^{6+}-$oxides, Sn_2WO_5 and Sn_3WO_6.

Experimental Section

Reagents. SnO (Alfa Aesar, 99%), WO_3 (Aldrich, 99+%), NaOH (Merck, 97%), and NH_4OH (Merck, 27%) were used as received.

Syntheses. To prepare Sn_2WO_5, SnO (0.350 g, 2.60×10^{-3} mol) and WO_3 (0.340 g, 1.47×10^{-3} mol) were added to either a NaOH (1M, 5 mL) or NH_4OH solution (27%, 5 mL). To prepare Sn_3WO_6, SnO (0.350 g, 2.60×10^{-3} mol) and WO_3 (0.115 g, 0.496×10^{-3} mol) were combined with the same solutions. The respective solutions were placed in a 23 mL Teflon-lined autoclave and held for 4 days at 220 °C. This was followed by slow cooling to room temperature at a rate of 6 °C h^{-1}. The mother liquor was decanted from the products that were then washed with water and ethanol. Yellow needle-shaped crystals and thin yellow plate-shaped crystals of Sn_2WO_5 and Sn_3WO_6, respectively, were recovered. The yields in NaOH solution of 5 and 10% for Sn_2WO_5 and Sn_3WO_6, respectively, were markedly improved when the reactions were performed in NH_4OH. In NH_4OH, the yields for Sn_2WO_5 and Sn_3WO_6 were 20 and 60%, respectively. All yields are based on SnO.

Numerous attempts to synthesize pure, polycrystalline Sn_2WO_5 were not successful. Various synthetic attempts using stoichiometric amounts of SnO and WO_3 at different temperatures and heating and cooling rates always produced a mixture of SnO_2, α-$SnWO_4$, and an unknown phase. We were able to synthesize pure, polycrystalline Sn_3WO_6 by standard solid-state techniques. A stoichiometric mixture of SnO (0.500 g, 3.71×10^{-3} mol) and WO_3 (0.2867 g, 1.24×10^{-3} mol) was ground with an agate mortar and pestle and introduced into a fused silica tube that was subsequently evacuated and sealed. The tube was heated to 540 °C for 40 h and then quenched to room temperature in ice water. If the tube is not quenched, but cooled to room temperature, Sn_3WO_6 is found as part of a mixture with α-$SnWO_4$. The powder X-ray diffraction pattern on the resultant yellow powder is in good agreement with the generated pattern from the single-crystal data (see Supporting Information).

Table 1. Crystallographic Data for Sn_2WO_5 and Sn_3WO_6

formula	Sn_2WO_5	Sn_3WO_6
fw	501.23	635.92
space group	$P2_1/n$	$C2/c$
a (Å)	7.994(2)	12.758(3)
b (Å)	13.712(4)	8.0838(16)
c (Å)	10.383(3)	13.865(3)
β (deg)	110.507(3)	112.49(3)
V (Å^3)	1066.0(5)	1321.2(5)
Z	4	8
T (K)	293.0(2)	293.0(2)
λ (Å)	0.71073	0.71073
ρ_{calcd} (g cm^{-3})	6.246	6.394
μ (mm^{-1})	30.76	28.54
$R(F)^a$	0.0553	0.0386
$R_w(F_o^2)^b$	0.1544	0.1048

^{a} $R(F) = \sum||F_o| - |F_c||/\sum|F_o|$. ^{b} $R_w(F_o^2) = [\sum w(F_o^2 - F_c^2)^2/\sum w(F_o^2)^2]^{1/2}$.

Single-Crystal X-ray Diffraction. For Sn_3WO_6 and Sn_2WO_5, a yellow needle-shaped ($0.01 \times 0.02 \times 0.21$ mm^3) crystal and a yellow plate-shaped ($0.03 \times 0.10 \times 0.14$ mm^3) crystal, respectively, were used for single-crystal data collection. Data were collected using a Siemens SMART APEX diffractometer equipped with a 1K CCD area detector using graphite-monochromated Mo Kα radiation. A hemisphere of data was collected using a narrow-frame method with scan widths of 0.50° in ω and an exposure time of 20 s per frame. The first 50 frames were remeasured at the end of the data collection to monitor instrument and crystal stability. The maximum correction applied to the intensities was <1%. The data were integrated using the Siemens SAINT program,[24] with the intensities corrected for Lorentz polarization, air absorption, and absorption attributable to the variation in the path length through the detector face plate. ψ-scans or SADABS calculations were used for the absorption correction on the hemisphere of data. The data were solved and refined using SHELXS-97 and SHELXL-97, respectively.[25,26] For Sn_2WO_5, all of the atoms, except for the oxygen atoms, were refined anisotropically, whereas for Sn_3WO_6, all of the atoms were refined anisotropically. With both refinements, the data converged for $I > 2\sigma(I)$. All calculations were performed using the WinGX-98 crystallographic software package.[27] Crystallographic data and selected bond distances for Sn_3WO_6 and Sn_2WO_5 are given in Tables 1−3, with additional details found in the Supporting Information.

Powder Diffraction. The X-ray powder diffraction data were collected on a Scintag XDS2000 diffractometer, equipped with Peltier germanium solid-state detector, at room temperature (Cu

(14) Lefebvre, I.; Lannoo, M.; Allan, G.; Ibanez, A.; Fourcade, J.; Jumas, J. C. *Phys. Rev. Lett.* **1987**, *59*, 2471.
(15) Lefebvre, I.; Szymanski, M. A.; Olivier-Fourcade, J.; Jumas, J. C. *Phys. Rev. B* **1998**, *58*, 1896.
(16) Watson, G. W.; Parker, S. C. *J. Phys. Chem. B* **1999**, *103*, 1258.
(17) Watson, G. W.; Parker, S. C.; Kresse, G. *Phys. Rev. B* **1999**, *59*, 8481.
(18) Seshadri, R.; Hill, N. A. *Chem. Mater.* **2001**, *13*, 2892.
(19) Waghmare, U. V.; Spaldin, N. A.; Kandpal, H. C.; Seshadri, R. *Phys. Rev. B* **2003**, *67*, 12511−12511.
(20) Stoltzfus, M. W.; Woodward, P.; Seshadri, R.; Park, J.-H.; Bursten, B. *Inorg. Chem.* **2007**, *46*, 3839.
(21) Halasyamani, P. S. *Chem. Mater.* **2004**, *16*, 3586.
(22) Jeitschko, W.; Sleight, A. W. *Acta Crystallogr.* **1972**, *B28*, 3174.
(23) Jeitschko, W.; Sleight, A. W. *Acta Crystallogr.* **1974**, *B30*, 2088.
(24) *SAINT*, 4.05 ed.; Siemens Analytical X-ray Systems, Inc.: Madison, WI, 1995.
(25) Sheldrick, G. M. *SHELXS-97, A Program for Automatic Solution of Crystal Structures*; University of Göttingen: Göttingen, Germany, 1997.
(26) Sheldrick, G. M. *SHELXL-97, A Program for Crystal Structure Refinement*; University of Göttingen: Göttingen, Germany, 1997.
(27) Farrugia, L. J. *J. Appl. Crystallogr.* **1999**, *32*, 837.

Table 2. Atomic Coordinates for Sn_2WO_5

atom	*x*	*y*	*z*	U_{eq} (Å^2)[a]
W(1)	0.74639(12)	0.33246(7)	1.46631(8)	0.0091(3)
W(2)	0.54332(12)	0.17486(7)	0.60450(8)	0.0084(3)
Sn(1)	0.6119(2)	0.10140(13)	1.30082(15)	0.0153(4)
Sn(2)	0.6834(2)	0.39908(13)	0.77270(16)	0.0147(4)
Sn(3)	0.7249(2)	0.14814(12)	0.95630(15)	0.0130(4)
Sn(4)	0.5581(2)	0.34842(13)	1.11084(15)	0.0127(4)
O(1)	0.979(2)	0.2869(12)	1.4937(15)	0.012(3)[b]
O(2)	0.629(2)	0.2625(12)	1.2924(15)	0.014(3)
O(3)	0.848(2)	0.3869(11)	1.6509(14)	0.006(3)
O(4)	0.755(2)	0.1814(12)	0.5621(15)	0.013(3)
O(5)	0.738(2)	0.4377(13)	1.3809(16)	0.022(4)
O(6)	0.313(2)	0.2188(12)	0.5819(16)	0.015(3)
O(7)	0.656(2)	0.2425(12)	0.7750(14)	0.011(3)
O(8)	0.446(2)	0.1209(11)	0.4226(15)	0.010(3)
O(9)	0.538(2)	0.3245(11)	1.5152(15)	0.012(3)
O(10)	0.556(2)	0.0671(13)	0.6944(16)	0.019(4)

[a] U_{eq} is defined as one-third of the trace of the orthogonalized U_{ij} tensor. [b] All oxygen atoms were refined isotropically.

Table 3. Atomic Coordinates for Sn_3WO_6

atom	*x*	*y*	*z*	U_{eq} (Å^2)[a]
W	0.07981(4)	0.63183(5)	0.09076(3)	0.0083(2)
Sn(1)	−0.16315(7)	0.84948(10)	0.11443(7)	0.0141(2)
Sn(2)	−0.15849(7)	0.43402(11)	0.12620(6)	0.0160(3)
Sn(3)	0.07806(7)	1.12610(9)	0.11644(7)	0.0124(2)
O(1)	0.0417(8)	0.8548(9)	0.0432(7)	0.0170(19)[b]
O(2)	−0.0613(7)	0.6412(10)	0.1206(7)	0.0161(19)
O(3)	0.1850(7)	0.6144(11)	0.0317(7)	0.0179(19)
O(4)	0.0466(7)	0.4017(11)	0.0783(7)	0.0169(17)
O(5)	0.1726(7)	0.6588(11)	0.2198(7)	0.0178(18)
O(6)	0.2111(7)	1.1390(10)	0.0598(7)	0.0144(18)

[a] U_{eq} is defined as one-third of the trace of the orthogonalized U_{ij} tensor. [b] All oxygen atoms were refined anisotropically.

Kα radiation, $\theta-\theta$ mode, flat-plate geometry) in the 2θ range of 10−60° with a step size and step time of 0.02° and 1 s, respectively.

Infrared and Raman Spectroscopy. Infrared spectra were recorded on a Matteson FTIR 5000 spectrometer in the 400−4000 cm^{-1} range, with the sample pressed between two KBr pellets. Raman spectra were recorded at room temperature with 100 mW laser power in which a Coherent 90−6 Ar^+ ion laser provided excitation radiation at 514.5 nm. Front scattering (135° illumination ample) geometry was used to collect the scattered photons from spinning solid samples in pressed KCl pellets. To improve the signal-to-noise ratio, multiple scans (2−4 scans) were collected and then averaged.

UV−vis Diffuse Reflectance Spectroscopy. UV−vis diffuse reflectance data for Sn_3WO_6 and Sn_2WO_5 were collected with a Varian Cary 500 scan UV−vis-NIR spectrophotometer over the spectral range of 200−1500 nm at room temperature. Poly(tetrafluoroethylene) was used as a reference material. Reflectance spectra were converted to absorbance with the Kubelka−Munk function.[28,29]

Thermogravimetric Analysis. Thermogravimetric analyses were carried out on a TGA 951 thermogravimetric analyzer (TA Instruments). The samples were contained within platinum crucibles and heated at a rate of 10 °C min^{-1} from room temperature to 800 °C in a nitrogen atmosphere.

Calculations. Electronic band structure calculations were carried out using version 47 of the Stuttgart tight bonding, linear muffin tin orbital, atomic sphere approximation (LMTO) code. LMTO is a self-consistent density functional theory code, which incorporates scalar-relativistic corrections. Detailed descriptions of the ab initio calculations are given elsewhere.[30,31] The effects of exchange and correlation were approximated using the Perdew−Wang generalized gradient approximation.[32]

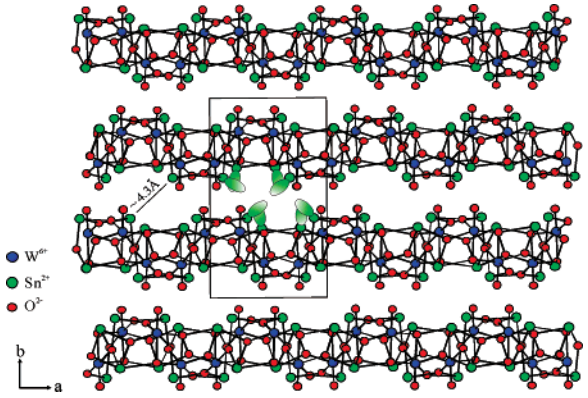

Figure 1. Ball-and-stick representation of Sn_2WO_5 in the *ab*-plane is shown. The lone pairs on the Sn^{2+} cations (green ovals) are shown schematically. Note that the closest $Sn^{2+}-Sn^{2+}$ interlayer distance is ~4.3 Å.

Results

Both Sn_2WO_5 and Sn_3WO_6 exhibit two-dimensional structural topologies, consisting of W_2O_{10} "clusters" linked to SnO_3 and SnO_4 polyhedra. For Sn_2WO_5, the layers are not completely flat (see Figure 1). The stereoactive lone-pair on Sn^{2+} points into the interlayer gap, resulting in the closest $Sn^{2+}-Sn^{2+}$ distance of ~4.3 Å. The layer itself is composed of two edge-shared WO_6 octahedra that are further connected to SnO_3 and SnO_4 polyhedra (see Figure 2). Each WO_6 octahedron is connected along the $\pm a$-axis to a SnO_4 polyhedron. Thus "double chains" of WO_6 and SnO_4 groups are observed. These double-chains are connected to each other, along the $\pm c$-axis, through the SnO_3 polyhedra (see Figure 2). The distance between the double chains is approximately 3.4 Å.

Sn_2WO_5 has two crystallographically unique W^{6+} cations and four unique Sn^{2+} cations. The W^{6+} cations are in an octahedral coordination environments bonded to six oxygen atoms, with W−O bond distances ranging from 1.683(18) to 2.288(16) Å. Both cations are displaced toward a vertex, local C_4 direction, resulting in one "short", one "long", and four "normal" W−O bonds. With the Sn^{2+} cations, two types of asymmetric coordination environments are observed. Two distorted trigonal pyramidal SnO_3 polyhedra are observed, as are two SnO_4 groups exhibiting a "seesaw" geometry. Both of these asymmetric coordination environments can be attributed to the stereoactive lone pair on the Sn^{2+} cation. The Sn−O bond distances range from 2.125(15) to 2.388(16) Å. Bond valence calculations[33,34] on Sn_2WO_5 resulted in values of 6.21 and 6.30 for W^{6+} and values ranging from 1.83 to 2.03 for Sn^{2+}.

Sn_3WO_6 also exhibits a layered topology. With this material, the layers are slightly more flat than those of

(28) Tauc, J. *Mat. Res. Bull*. **1970**, *5*, 721.
(29) Kubelka, P.; Munk, F. *Tech. Phys*. **1931**, *12*, 593.
(30) Anderson, O. K. *Phys. Rev. B* **1975**, *12*, 3060.
(31) Anderson, O. K.; Jepsen, O. *Phys. Rev. Lett*. **1984**, *53*, 2571.
(32) Perdew, J. P.; Wang, Y. *Phys. Rev. B* **1986**, *33*, 8800.
(33) Brown, I. D.; Altermatt, D. *Acta Crystallogr*. **1985**, *B41*, 244.
(34) Brese, N. E.; O'Keeffe, M. *Acta Crystallogr*. **1991**, *B47*, 192.

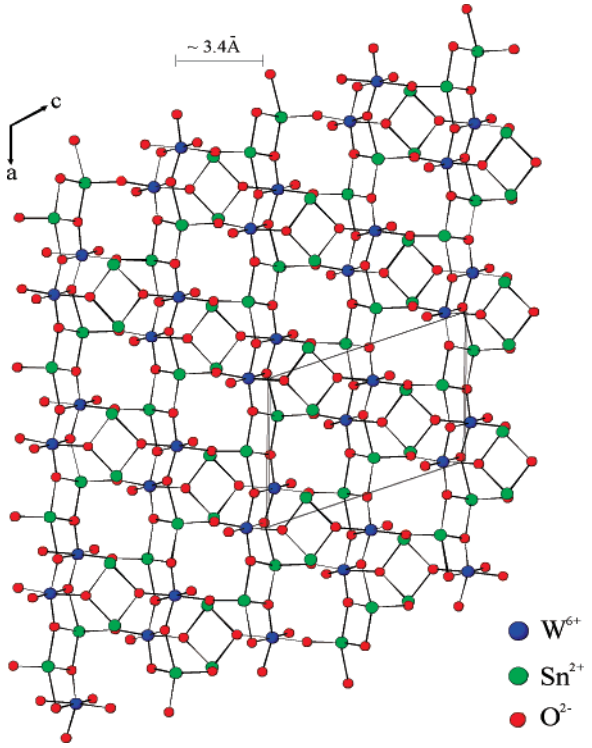

Figure 2. Ball-and-stick representation of Sn_2WO_5 in the *ac*-plane is shown. Note that both SnO_3 and SnO_4 polyhedra are observed.

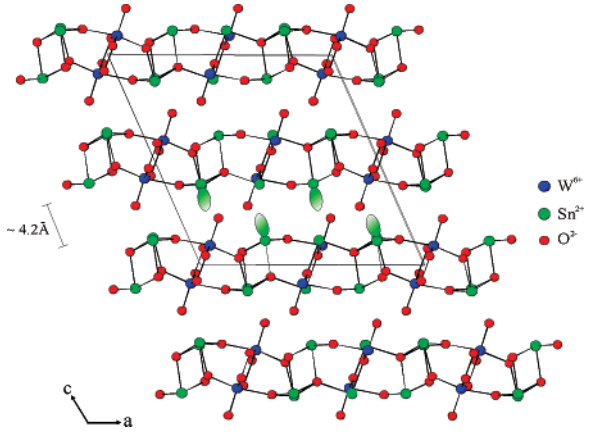

Figure 3. Ball-and-stick representation of Sn_3WO_6 in the *ac*-plane is shown. The lone pairs on the Sn^{2+} cations (green ovals) are shown schematically. Note that the closest $Sn^{2+}-Sn^{2+}$ interlayer distance is ~4.2 Å.

Sn_2WO_5. Similar to Sn_2WO_5, the lone-pair on the Sn^{2+} cation points toward the interlayer space (see Figure 3). In addition, one of the oxide ligands on W^{6+} also points into the interlayer space. An interlayer separation of ~4.2 Å is observed. The layers in Sn_3WO_6 are composed of two edge-shared WO_6 octahedra that are further connected to SnO_3 and SnO_4 polyhedra. Each WO_6 octahedron is connected along the $\pm b$-axis to a SnO_4 polyehdra. Thus, as with Sn_2WO_5, double chains of WO_6 and SnO_4 groups are observed. These double chains are connected to each other, along the $\pm a$-axis, through two SnO_3 polyhedra (see Figure 4). Although both Sn_2WO_5 and Sn_3WO_6 exhibit W_2O_{10} clusters, there is an additional "SnO" unit in Sn_3WO_6. The connectivity of this unit may be written as $[Sn_2O_{3/3}O_{2/2}]^0 \rightarrow Sn_2O_2 \rightarrow SnO$. The addition of this SnO unit increases the distance between the double-chains to ~6.4 Å.

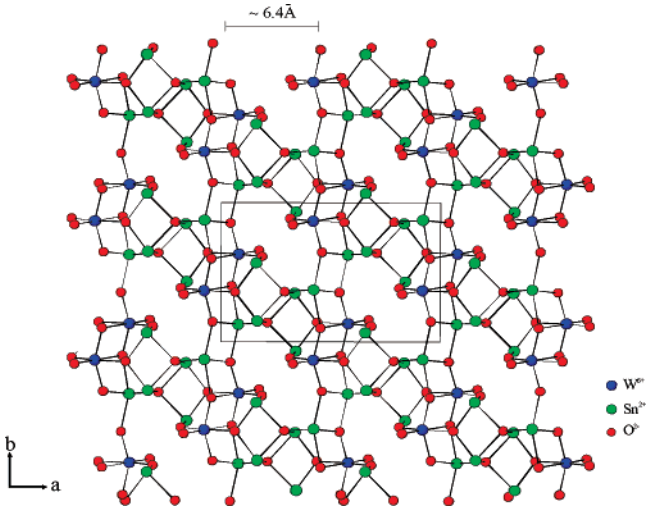

Figure 4. Ball-and-stick representation of Sn_3WO_6 in the *ac*-plane is shown. Note that both SnO_3 and SnO_4 polyhedra are observed.

Sn_3WO_6 has one unique W^{6+} cation and three unique Sn^{2+} cations. The W^{6+} cation is in an octahedral coordination environment, bonded to six oxygen atoms with W−O distances ranging from 1.741(9) to 2.297(9)Å. Similar to Sn_2WO_5, the cation is displaced toward a vertex, local C_4 distortion, resulting in one short, one long, and four normal W−O bonds. The coordination environments of the Sn^{2+} cation are also similar to those of Sn_2WO_5. For the three unique Sn^{2+} cations, two distorted trigonal pyramidal SnO_3 polyhedra, and one SnO_4 group in a "seesaw" geometry are observed. The Sn−O bond distances range from 2.103(8) to 2.278(8) Å. Bond valence calculations[33,34] on Sn_3WO_6 resulted in a value of 6.17 for W^{6+} and in values ranging from 1.67 to 2.08 for Sn^{2+}.

Infrared and Raman Spectroscopy. The infrared and Raman spectra of Sn_3WO_6 and Sn_2WO_5 revealed W−O, Sn−O, and W−O−Sn vibrations. W−O vibrations are observed in both IR and Raman spectra and occur between 600 and 950 cm^{-1}. Sn−O vibrations are also observed in the Raman spectra and are found around 0−250 cm^{-1} as multiple bands. W−O−Sn vibrations are observed between 300 and 600 cm^{-1}. The assignments were done on the basis of the Raman data for the previously reported $SnWO_4$ structures.[35] The assignments of infrared and Raman vibrations for Sn_3WO_6 and Sn_2WO_5 are listed in Table 5.

UV−Vis Diffuse Reflectance Spectroscopy. The UV−vis diffuse reflectance spectra for Sn_2WO_5 and Sn_3WO_6 have been deposited in the Supporting Information. Absorption (K/S) data were calculated from the Kubelka−Munk function[29]

$$F(R) = \frac{(1-R)^2}{2R} = \frac{K}{S}$$

Here R represents the reflectance, K the absorption, and S the scattering. In a (K/S) versus E (eV) plot,[28] extrapolation of the linear part of the rising curve to zero provides the

(35) Solis, J. L.; Frantti, J.; Lantto, V.; Haggstrom, L.; Wikner, M. *Phys. Rev. B* **1998**, *57*, 13491.

Table 4. Selected Bond Distances (Å) for Sn_2WO_5 and Sn_3WO_6

	Sn_2WO_5[a]		
W(1)−O(9)	1.909(16)	Sn(1)−O(3)$^{\#3}$	2.143(15)
W(1)−O(5)	1.683(18)	Sn(1)−O(2)	2.217(17)
W(1)−O(4)$^{\#1}$	2.288(16)	Sn(2)−O(8)$^{\#4}$	2.149(15)
W(1)−O(3)	1.949(14)	Sn(2)−O(7)	2.159(16)
W(1)−O(2)	1.968(15)	Sn(2)−O(3)$^{\#2}$	2.129(14)
W(1)−O(1)	1.886(16)	Sn(3)−O(9)$^{\#5}$	2.388(16)
W(2)−O(10)	1.731(17)	Sn(3)−O(7)	2.190(15)
W(2)−O(9)$^{\#2}$	2.246(15)	Sn(3)−O(6)$^{\#4}$	2.209(17)
W(2)−O(8)	1.921(15)	Sn(3)−O(1)$^{\#3}$	2.311(15)
W(2)−O(7)	1.920(15)	Sn(4)−O(6)$^{\#4}$	2.348(16)
W(2)−O(6)	1.874(17)	Sn(4)−O(4)$^{\#6}$	2.332(16)
W(2)−O(4)	1.893(16)	Sn(4)−O(2)	2.125(15)
Sn(1)−O(8)$^{\#1}$	2.145(14)	Sn(4)−O(1)$^{\#3}$	2.187(16)
	Sn_3WO_6[b]		
W(1)−O(5)	1.741(9)	Sn(1)−O(6)$^{\#3}$	2.261(8)
W(1)−O(4)	1.901(9)	Sn(2)−O(2)	2.103(8)
W(1)−O(4)$^{\#1}$	2.297(9)	Sn(2)−O(3)$^{\#1}$	2.120(9)
W(1)−O(3)	1.826(8)	Sn(2)−O(6)$^{\#3}$	2.278(8)
W(1)−O(2)	1.996(8)	Sn(3)−O(1)	2.386(8)
W(1)−O(1)	1.917(8)	Sn(3)−O(1)$^{\#2}$	2.161(9)
Sn(1)−O(2)	2.109(8)	Sn(3)−O(4)$^{\#4}$	2.289(9)
Sn(1)−O(6)$^{\#2}$	2.256(8)	Sn(3)−O(6)	2.127(9)

[a] Symmetry transformations used to generate equivalent atoms: #1 $x, y, z+1$; #2 $x, y, z-1$; #3 $x-1/2, -y+1/2, z-1/2$; #4 $x+1/2, -y+1/2, z+1/2$; #5 $x+1/2, -y+1/2, z-1/2$; #6 $x-1/2, -y+1/2, z+1/2$. [b] Symmetry transformations used to generate equivalent atoms: #1 $-x, -y+1, -z$; #2 $-x, -y+2, -z$; #3 $x-1/2, y-1/2, z$; #4 $x, y+1, z$.

Table 5. Infrared and Raman Data (cm^{-1}) for Sn_2WO_5 and Sn_3WO_6

Sn_2WO_5			Sn_3WO_6		
W−O	Sn−O	W−O−Sn	W−O	Sn−O	W−O−Sn
		Raman (cm^{-1})			
917	238	433	887	180	439
883	222	375	777	69	344
753	194	355	750		
668	78				
		IR (cm^{-1})			
922		556	889		587
889		411	784		539
764			668		458
667					

onset of absorption at 2.59 and 2.49 eV for Sn_2WO_5 and Sn_3WO_6, respectively. The overall band gap for each material may be attributable to the degree of W (5d) orbitals that are engaged in the conduction bands, as well as the distortions arising from SnO_3 and SnO_4 polyhedra (see Supporting Information).

Thermogravimetric Analysis. The thermal behavior of Sn_2WO_5 and Sn_3WO_6 was investigated using thermogravimetric analysis. These two compounds are stable up to 800 °C in a nitrogen atmosphere (see Supporting Information). In air, however, both Sn_2WO_5 and Sn_3WO_6 decompose to a mixture of SnO_2 and WO_3.

Calculations. The band structure calculations predict band gaps of 1.3 eV for Sn_2WO_5 and 1.2 eV for Sn_3WO_6, which are considerably smaller than the experimental values of 2.59 and 2.49 eV. The tendency for electronic band structure calculations to underestimate the band gap energy has been well documented in previous studies.[36−38] Despite this shortcoming, the DFT calculations are effective in identifying the key orbital interactions and reproducing trends. The general features of the electronic structure for Sn_2WO_5 and Sn_3WO_6 are very similar, which is consistent with the experimental observation that these two compounds have similar band gaps. The valence band is composed of an antibonding Sn(5s)−O(2p) interaction with considerable mixing from the Sn(5p) orbitals. This is a classic example of a second-order Jahn−Teller distortion and is further evidence of the distorted environment on the SnO_3 and SnO_4 polyhedra. Stated in another way, we can say that the electronic states associated with the Sn^{2+} lone-pairs dominate the top of the valence band. The bottom of the conduction band is predominantly W(5d)−O(2p) antibonding in character.

Discussion

Before the electronic structures and properties of Sn_2WO_5 and Sn_3WO_6 are described, a brief review of the structural chemistry is useful. Although Sn_2WO_5 and Sn_3WO_6 crystallize in centrosymmetric space groups, both materials contain cations in asymmetric coordination environments. All of the W^{6+} cations are distorted from the center of their oxide octahedra toward a vertex. It is interesting to note that in oxides with octahedrally coordinated W^{6+} cations, a distortion toward a vertex is somewhat rare, occurring less than 15% of the time.[39] We may also discuss the distortions of the W^{6+} and Sn^{2+} cations with regard to primary and secondary distortive effects.[10,40] Briefly, with both the W^{6+} and Sn^{2+} cations, the primary distortive effect is attributable to SOJT effects, that is, electronic effects. The secondary distortive effect is caused by bond networks and lattice stresses, that, for our purposes are between the WO_6 and SnO_x ($x = 3$ or 4) polyhedra. In a previous article, we determined that in oxides containing d^0 transition metals and a lone-pair cation, the displacement of the d^0 transition metal is directed away from the oxide ligands that bridge to the lone-pair cation.[21] We suggested that the reason for the directionality of the distortion is attributable to the "predistorted" nature of the lone-pair polyhedra. In other words, if the d^0 transition metal cation were to distort toward an oxide ligand which bridges to a lone-pair cation, the lone-pair cation would also displace. But, since the lone-pair cation is already in an asymmetric coordination environment, any additional distortion would be unfavorable. Thus, the d^0 transition metal distorts away from any oxide ligands that bridge to a lone-pair cation. This is the situation with the W^{6+} cations in Sn_2WO_5 and Sn_3WO_6 (see Figure 5). With all three unique W^{6+} cations, the distortion is toward an oxide ligand that is not bonded to a lone-pair cation, that is, toward a vertex. In addition to the direction of the displacement, the extent, or magnitude of the distortion is also important.

(36) Eng, H. W.; Barnes, P. W.; Auer, B. M.; Woodward, P. *J. Solid State Chem.* **2003**, *175*, 94.
(37) Mizoguchi, H.; Eng, H. W.; Woodward, P. *Inorg. Chem.* **2004**, *43*, 1667.
(38) Mizoguchi, H.; Woodward, P. *Chem. Mater.* **2004**, *16*, 5233.
(39) Ok, K. M.; Halasyamani, P. S.; Casanova, D.; Llunell, M.; Alemany, P.; Alvarez, S. *Chem. Mater.* **2006**, *18*, 3176.
(40) Welk, M. E.; Norquist, A.; Arnold, F. P.; Stern, C. L.; Poeppelmeier, K. R. *Inorg. Chem.* **2002**, *41*, 5119.

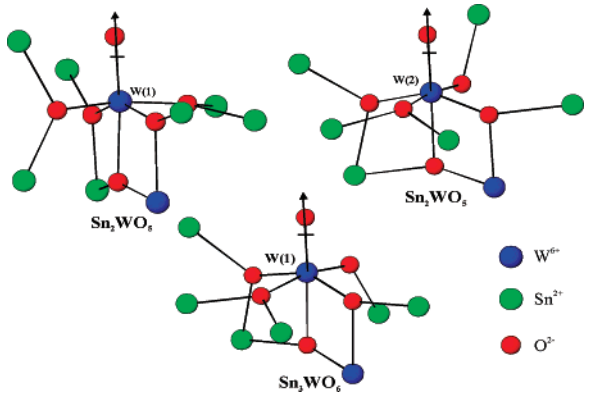

Figure 5. Ball-and-stick representation of the intraoctahedral distortion of W^{6+} in Sn_2WO_5 and Sn_3WO_6 is shown. Note for both compounds, the W^{6+} cation is displaced toward a vertex of its WO_6 octahedron.

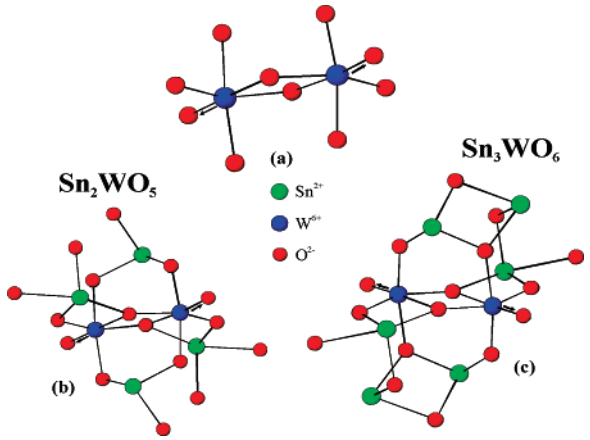

Figure 6. Ball-and-stick representation of the (a) W_2O_{10} cluster common to both Sn_2WO_5 and Sn_3WO_6, and SnO_3 and SnO_4 polyhedra associated with (b) Sn_2WO_5 and (c) Sn_3WO_6. The black arrows represent the direction of the W^{6+} intraoctahedral distortion.

Recently, we published an article[39] that describes using continuous symmetry measures[41−43] to better quantify the magnitude of the distortion of the d^0 transition metal. Using this methodology with the SHAPE program,[44] we determined that for Sn_2WO_5 the magnitudes of the W(1) and W(2) distortions are 0.077 and 0.096 Å^2, respectively, whereas for Sn_3WO_6 the magnitude of the W(1) distortion is 0.111 Å.^{2} The distortions are somewhat larger than the previously reported average for W^{6+} of 0.065 Å.[239] The Sn^{2+} cations are also in asymmetric coordination environments, attributable to their stereoactive lone pair, bonded to three or four oxygen atoms. The asymmetric W^{6+} and Sn^{2+} coordination environments result in local dipole moments for the WO_6, SnO_3, and SnO_4 polyhedra. The magnitudes of the W^{6+} and Sn^{2+} distortion may also be quantified by determining the local dipole moments. The method has been described earlier[45,46] and uses a bond-valence approach to calculate the magnitude of the local dipole moments. We have extended this approach to include lone-pair polyhedra.[47−49] With the lone-pair polyhedra, the lone pair is given a charge of −2 and is localized 0.95 Å from the Sn^{2+} cation. This Sn^{2+}−lone pair distance is based on earlier work by Galy et al.[50] Using this approach, the dipole moment for the SnO_3 and SnO_4 polyhedra are in the opposite direction of the lone pair. We have calculated the dipole moment for the WO_6, SnO_3, and SnO_4 polyhedra in Sn_2WO_5 and Sn_3WO_6 (see Table 6). For comparison, we have also calculated the dipole moment for the same polyhedra in the other reported Sn^{2+} d^0 oxides, α,β-$SnWO_4$.

Table 6. Calculation of Dipole Moments for Sn_2WO_5, Sn_3WO_6, α-$SnWO_4$, and β-$SnWO_4$

compound	distortion symmetry, species	dipole moment
Sn_2WO_5	C_4, $W(1)O_6$	1.9
	C_4, $W(2)O_6$	2.3
	$Sn(1)O_3$	6.8
	$Sn(2)O_3$	7.2
	$Sn(3)O_4$	7.1
	$Sn(4)O_4$	6.1
Sn_3WO_6	C_4, $W(1)O_6$	3.4
	$Sn(1)O_3$	6.2
	$Sn(2)O_3$	7.1
	$Sn(3)O_4$	7.4
α-$SnWO_4$	C_2, $W(1)O_6$	2.4
	$Sn(1)O_4$	6.0
β-$SnWO_4$	WO_4 tetrahedron	0.52
	$Sn(1)O_3$	5.1

Although the W^{6+} cations in Sn_2WO_5 and Sn_3WO_6 are displaced in the same direction, toward a vertex, the magnitude of their distortion varies greatly. The W^{6+} distortions in Sn_2WO_6 are 15−30% *larger* than those of Sn_3WO_5. As stated earlier, a common unit found in both reported compounds is a W_2O_{10} cluster (see Figure 6a). One of the differences between Sn_2WO_5 and Sn_3WO_6 is an additional SnO unit in the latter. This difference becomes apparent when we examine the SnO_x polyhedra around the W_2O_{10} cluster in both compounds (see Figure 6b and c). As seen in Figure 6b and c, there is an additional SnO_3 polyhedron associated with the W_2O_{10} cluster in Sn_3WO_6. We suggest that although the SnO_3 and SnO_4 polyhedra are predistorted, that is, in an asymmetric coordination environment attributable to their stereoactive lone pair, the additional SnO_3 polyhedron in Sn_3WO_6 provides structural flexibility for the associated W_2O_{10} cluster. This additional structural flexibility manifests itself through a larger intraoctahedral distortion of the W^{6+} in Sn_3WO_6 compared with that in Sn_2WO_5.

To further analyze the distortions occurring in Sn_2WO_5 and Sn_3WO_6, electronic density of states plots (DOS) were calculated in the experimentally observed structures, as well as a more symmetric environment used by the SHAPE program.[44] We begin our discussion by analyzing the DOS of Sn_2WO_5 and Sn_3WO_6 with the WO_6 octahedron in a symmetric environment, that is, six nearly equivalent W−O bonds with lengths ranging from 1.9−2.0 Å and O−W−O

(41) Zabrodsky, H.; Peleg, S.; Avnir, D. *J. Am. Chem. Soc.* **1992**, *114*, 7843.
(42) Alvarez, S.; Avnir, D.; Llunell, M.; Pinsky, M. *New J. Chem.* **2002**, *26*, 996−1009.
(43) Alvarez, S.; Alemany, P.; Casanova, D.; Cirera, J.; Llunell, M.; Avnir, D. *Coord. Chem. Rev.* **2005**, *249*, 1693.
(44) Llunell, M.; Casanova, D.; Cirera, J.; Bofill, J. M.; Alemany, P.; Alvarez, S.; Pinsky, M.; Avnir, D. *SHAPE Program*, version 1.1: University of Barcelona: Barcelona, Spain, 2004.
(45) Maggard, P. A.; Nault, T. S.; Stern, C. L.; Poeppelmeier, K. R. *J. Solid State Chem.* **2003**, *175*, 25.
(46) Izumi, H. K.; Kirsch, J.; Stern, C. L.; Poeppelmeier, K. R. *Inorg. Chem.* **2005**, *44*.
(47) Ok, K. M.; Halasyamani, P. S. *Inorg. Chem.* **2005**, *44*, 3919.
(48) Ok, K. M.; Halasyamani, P. S. *Inorg. Chem.* **2005**, *44*, 9353.
(49) Ok, K. M.; Halasyamani, P. S. *J. Solid State Chem.* **2006**, *179*, 1345.
(50) Galy, J.; Meunier, G. *J. Solid State Chem.* **1975**, *13*, 142.

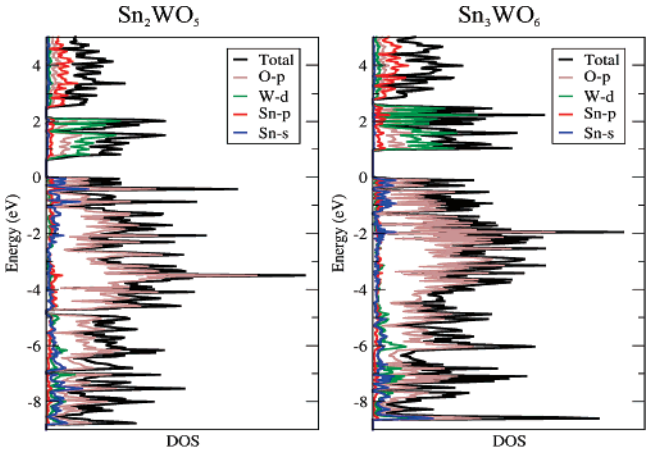

Figure 7. On the left, the electronic density of states, shown in black, as calculated for Sn_2WO_5 with a symmetric WO_6 octahedron environment. On the right, the electronic density of states, shown in black, as calculated for Sn_3WO_6 with a symmetric WO_6 octahedron environment. For both figures, partial density of states curves for O(2p), W(5d), Sn(5p), and Sn(5s) contributions are shown in gray, green, red, and blue, respectively.

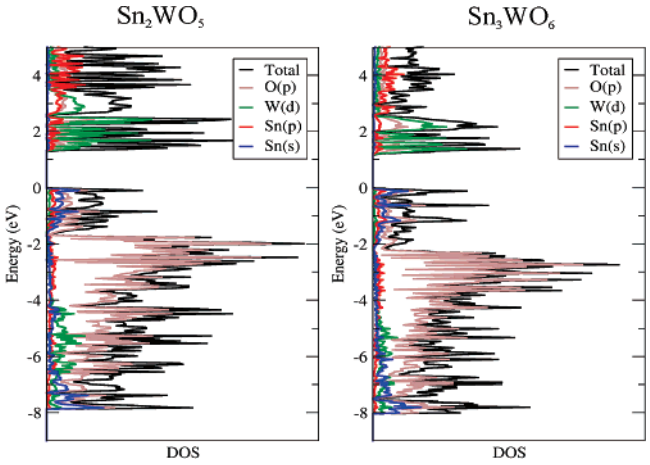

Figure 8. On the left, the electronic density of states, shown in black, as calculated for the experimentally observed Sn_2WO_5 with a distorted WO_6 octahedron environment. On the right, the electronic density of states, shown in black, as calculated for the experimentally observed Sn_3WO_6 with a distorted WO_6 octahedron environment. Partial density of states curves for O(2p), W(5d), Sn(5p), and Sn(5s) contributions are shown in gray, green, red, and blue, respectively.

angles of approximately 90 and 180°. The DOS for the symmetric environments are shown in Figure 7 with Sn(s), Sn(p), W(d), and O(p) contributions in blue, red, green, and gray respectively. The electronic structures for both compounds in these hypothetical structures are very similar to each other. In both cases, the lower portion of the valence band (−9 to −5 eV) is composed of predominantly O(2p) bonding character resulting from Sn(5s)−O(2p) and W(5d)−O(2p) bonding interactions. The middle region (−5 to −1 eV) is primarily O(2p) nonbonding, while the top region (−1 to 0 eV) near the Fermi level has an electronic structure which is consistent with a lone pair distortion. This interaction not only consists of Sn(5s)−O(2p) antibonding states, but there is also a considerable amount of Sn(5p) mixing, indicative of a SOJT distortion. The lower-energy region of the conduction band (+1 to 2.5 eV) is composed of W(5d)−O(2p) antibonding interactions. At higher energies (+3 to +6 eV), the Sn(5p) states make the largest contribution. There is a small but distinct separation between the two.

Now we focus our attention to the DOS of the experimentally observed structures for Sn_2WO_5 and Sn_3WO_6 (see Figure 8). In these structures, the tungsten distorts toward a vertex, and this distortion has several consequences on the electronic structure. The general characteristics of the valence band have not changed; however, analysis of the integrated density of states at the bottom of the valence band shows increases in the W−O bonding character of 8.3 and 8.5% for Sn_2WO_5 and Sn_3WO_6, respectively. There are also noticeable changes, particularly in the conduction band states that arise from W(5d) and O(2p) antibonding interactions. A distortion toward the vertex lowers symmetry of the WO_6 polyhedron from pseudo-O_h to C_4, which removes the degeneracy of the t_{2g} and e_g orbitals. In doing so, tungsten forms a stronger bond to oxygen that destabilizes the antibonding W(5d)−O(2p) states sufficiently to eliminate the distinct separation in energy between the W(5d) and Sn(5p) states. The band gaps following the distortion increase slightly from 1.0 to 1.3 eV for Sn_2WO_5 and 0.7 to 1.2 eV for Sn_3WO_6, which is consistent with the fact that an out-of-center distortion depends inversely on the energy gap between the HOMO and LUMO states. In addition, the relative energies of the Sn_2WO_5 and Sn_3WO_6 are stabilized by 1.4 and 0.9 eV, respectively, upon distortion.

Conclusion

We have demonstrated that new $Sn^{2+}-d^0-$oxides may be synthesized through a mild hydrothermal technique. Specifically, Sn_2WO_5 and Sn_3WO_6 have been synthesized and represent only the third and fourth reported $Sn^{2+}-d^0-$ oxide. Both materials contain cations, Sn^{2+} and W^{6+}, in asymmetric coordination environments attributable to second-order Jahn−Teller effects. With the W^{6+} cation, an out-of-center distortion is observed toward a vertex, that is, a corner-type distortion. The displacement is also away from the oxide ligands bridging to the Sn^{2+} cations. The magnitudes of the distortions range from 0.077 to 0.111 Å^2, which is slightly larger than the previously reported average of 0.065 Å.^{2} With Sn^{2+}, a stereoactive lone pair is observed that results in an asymmetric coordination environment. Through LMTO calculations, we were able to determine that the lone pair is attributable to Sn 5s, 5p, and O 2p interactions. We were also able to determine, through the calculations, that the out-of-center distortion slightly stabilizes the W−O bonding states, confirming the experimental structure.

Acknowledgment. P.S.H., H.Y.C., K.M.O., and J.H.K. thank the Robert A. Welch Foundation and the NSF-Career Program (DMR-0092054) for support. The authors also acknowledge funding from the NSF through their support of the Center for the Design of Materials (CHE-043567).

Supporting Information Available: Crystallographic data in CIF format, X-ray diffraction pattern, IR, Raman,and UV−vis spectra, and thermogravimetric data. This material is available free of charge via the Internet at http://pubs.acs.org.

IC700740M